Structure and Dynamics of Confined Water in $AlPO_4$-5 Zeolite

N. Floquet,*,† J. P. Coulomb,† N. Dufau,‡ and G. Andre§

C.R.M.C.-N. − CNRS, Campus de Luminy, Case 901, 13288 Marseille Cedex 9, France, MADIREL − UMR 6121, Centre de St Jérome, 13397 Marseille Cedex 20, France, and Laboratoire Léon − Brillouin, CEA, Saclay, 91191 Gif-sur-Yvette, Saclay, France

Received: March 24, 2004; In Final Form: June 2, 2004

The structural and dynamic properties of confined water in $AlPO_4$-5 zeolite (Ø = 7.3 Å) have been investigated by neutron scattering experiments during the adsorption process. Our aim is to elucidate the peculiar behavior of confined water at the nanoscopic confinement range. Confined water presents unusual properties in comparison with other sorbate species such as deuterium or methane. Even in the nanoporous diameter range, the water sorption phenomenon looks like the so-called "capillary condensation" phase transition or the "dry−wet" transition. Furthermore, the sorbed water quantity in $AlPO_4$-5 channels is exceptionally large. Our structural and dynamic results clearly show that the so-called "capillary condensation" step observed in the sorption isotherm is the signature of a crystallization phenomenon at room temperature (T = 300 K). It corresponds to the growth of two helices of ice of high density (d = 1.2) that is driven by structural commensurability with the $AlPO_4$-5 channel structure.

1. Introduction

Due to its major importance in several scientific domains (biology, geology, climatology), the structural and dynamics properties of water confined in porous media (clays, coals, zeolite, porous glasses, etc.) have been intensively investigated. Numerous studies are devoted to the water-confined phase in mesoporous molecular sieves, such as porous Vycor glass, MCM-41, and SBA-15.[1−9] Current interest mainly concerns the freezing and melting behavior of the mesoconfined water. Generally, their temperatures are always depressed as compared to those of the bulk.[6] Other studies are interested in water confined in nanoporous materials such as zeolites (VPI-5,[10−12] $AlPO_4$-5,[13−17] wairakite,[18] bikitaite,[19] etc.) and more recently carbon nanotubes.[20−22] In this case of confinement at the nanometer scale, a very interesting aspect of the research is the observation of the so-called "wet−dry transition" that involves a significant amount of water entering in the channel even when the channel wall is hydrophobic.[23]

The study of the sorption of water in $AlPO_4$-5 has been largely published.[13−17] As observed in Figure 1, the water sorption isotherm in $AlPO_4$-5 belongs to the type III isotherm. This originality of water sorption in $AlPO_4$-5 is outstanding when compared to sorption isotherms of other sorbate species. The last are usually of type I, as shown in Figure 1 for the sorption of methane and deuterium. What is also noticeable is the exceptionally large quantity of water sorbed in $AlPO_4$-5 as compared to that of a smaller molecule such as deuterium. The particularities of the water sorption behavior in $AlPO_4$-5 have been largely analyzed. In their extended study, Newalkar et al. interpreted the water condensation phenomenon as induced by the structural characteristics of the $AlPO_4$-5 framework porosity (Figure 2). The initial water sorption occurs in the secondary 6-membered ring channels, and then water fills the primary 12-membered ring channels via a condensation mechanism. Yet, actually there is no structural data to validate this water sorption mechanism. The structure of confined water in $AlPO_4$-5 has

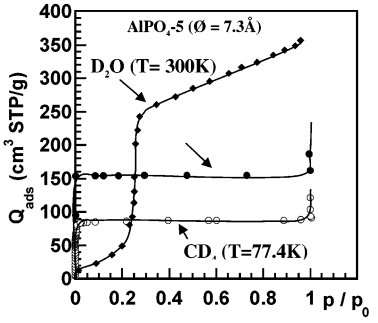

Figure 1. Adsorption isotherms on $AlPO_4$-5 (Ø = 7.3 Å) of water (◆), deuterium (●), and methane (○) at T = 300, 10, and 77.4 K, respectively.

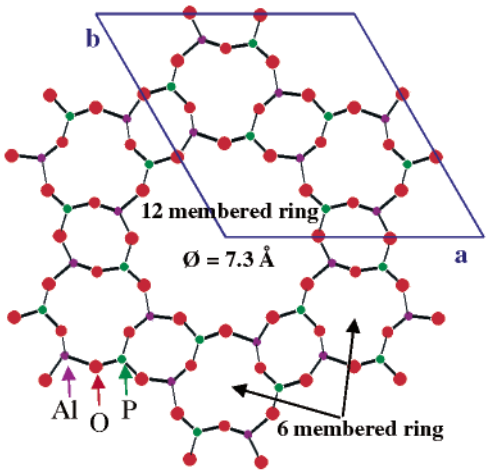

Figure 2. View along the c channel direction of the $AlPO_4$-5 hexagonal structure (a = 13.74 Å and c = 8.48 Å) showing the main 12-membered ring and the secondary 6-membered ring.

* Corresponding author. E-mail: floquet@crmcn.univ-mrs.fr.
† C.R.M.C.-N.
‡ MADIREL.
§ Laboratoire Léon.

10.1021/jp048687n CCC: $27.50
Published on Web 08/05/2004

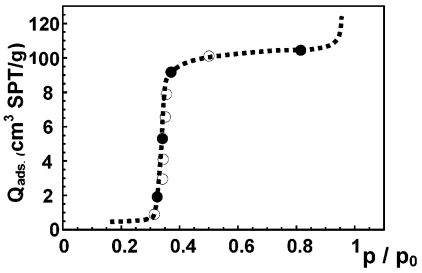

Figure 3. Calibration sorption isotherm measured at $T = 300$ K during the IQNS experiment concerning the $H_2O/AlPO_4$-5 system. The full circle (●) represents the water loading corresponding to the IQNS measurements.

not been determined even for a fully hydrated sample. Also, the structural determination of other fully hydrated zeolites such as VPI-5[10,11] and Linde L[24] was reported. In the present study, we investigated the structure and dynamics of water molecules during their sorption in $AlPO_4$-5 by neutron scattering in the temperature range 280−300 K. The detailed analysis of the experimental neutron data led us to locate the water molecules inside the $AlPO_4$-5 channels at each step of the sorption. Thus, our results confirm that the unusual sorption behavior of water is related to the structural characteristics of the $AlPO_4$-5 framework porosity. The so-called "capillary condensation" phenomenon corresponds to the growth of a dense ice, the structure of which is a double helix commensurate with the $AlPO_4$-5 channel structure. Our findings would extend the understanding of how water behaves on that nanoscale confinement.

2. Experimental Section

The $AlPO_4$-5 samples were synthesized in the Laboratoire des Matériaux Minéraux (Université de Haute Alsace, Mulhouse, France). Their physical characteristics (morphological aspect, high level of crystallinity, and highest sorption capacity) were largely measured.[25] Prior to any experiments (calibration isotherms or neutron scattering measurements), the sample was outgassed under vacuum ($P \leq 10^{-6}$ Torr) at $T = 400$ °C for about 12 h. The sample, weighing 1.163 g, was transferred to a cylindrical aluminum can mounted in a helium cryostat. The sample temperature was controlled to better than 0.1 K during the measurements. Research grade D_2O or H_2O gas was admitted to the sample through a homemade experimental system. The sorbed amounts were determined volumetrically with an accuracy of 1% in volume and 0.01 Torr in pressure.

Both adsorption and desorption isotherms with D_2O (or H_2O) were performed at $T = 300$ K in the neutron scattering cryostat. Besides their intrinsic interest, these isotherms were used to verify water loadings at various stages of the neutron experiments. The temperatures were controlled by the measure of the water-saturated vapor pressure P_o. A complete sorption isotherm was measured at $T = 300$ K for H_2O (Figure 3) and for D_2O (Figure 5).

The two-axis neutron diffractometer, G4-1, at the Leon Brillouin Laboratory was used for the elastic neutron scattering experiments. The G4-1 setup characteristics allow one to reach very large d spacings: the used wavelength is 2.4266 Å, and the instrumental resolution of the spectrometer is minimal at $2\Theta \leq 60°$. Besides, the G4-1 setup is well adapted to follow in situ adsorption experiments, the minimal acquisition time due to the high acquisition rate of the multidetector being of the order of 1 min.

Quasi-elastic neutron scattering measurements reported in recent papers[26,27] were done at the Leon Brillouin Laboratory using the inelastic time-of-flight spectrometer MIBEMOL. The recorded spectra came from the same $AlPO_4$-5 sample. Research grade H_2O gas was used, and the same experimental adsorption procedure was carried out for these experiments.

3. Results and Discussion

3.1. IQENS Results. Incoherent quasi-elastic neutron scattering (IQNS) spectra of the $H_2O/AlPO_4$-5 system were recorded at $T = 300$ K. Figure 3 gives the water sorption calibration isotherm and the H_2O loadings corresponding to the measured IQNS spectra shown in Figure 4a and b. There is no difference in the calibration isotherms measured at $T = 300$ K due to isotopic effects between H_2O and D_2O. The IQNS signal is proportional to the confined water loading. There is no quasi-elastic broadening of the signal above $Q_{ads} = 4$ H_2O/unit cell; the IQNS signal is a pure elastic line similar to the instrumental resolution. It is deduced that, at $T = 300$ K, the water molecular translational mobility D_t is quite small: up to $Q_{ads} = 4$ H_2O/unit cell, $D_t \leq 10^{-6}$ cm^2 s^{-1}, and above $Q_{ads} = 4$ H_2O/unit cell, $D_t \ll 10^{-6}$ cm^2 s^{-1}. It is concluded that the confined water phase in the $AlPO_4$-5 nanopore is an icy phase at $T = 300$ K. Thus, the melting temperature of the confined water in the $AlPO_4$-5 nanopore is displaced toward the high-temperature side, while in the MCM-41 mesopore it is displaced toward the low-temperature side ($T_{sol} = 230$ K for water confined in MCM-41 (Ø = 24 Å)).[4,6]

3.2. Neutron Diffraction Results. Neutron diffraction patterns of the $D_2O/AlPO_4$-5 system were recorded at $T = 300$ K. Figure 5 gives the water sorption calibration isotherm and the D_2O loadings corresponding to the recorded diffractograms. The vertical uptake step, called the "capillary condensation" step, begins at the loading $Q_{ads} = 4$ D_2O/unit cell (uc) and ends at $Q_{ads} = 16$ D_2O/uc. The full loading corresponds to 18 D_2O/uc. Diffractograms of the empty $AlPO_4$-5 and at D_2O loadings characterizing the adsorption isotherm steps are plotted in Figure 6.

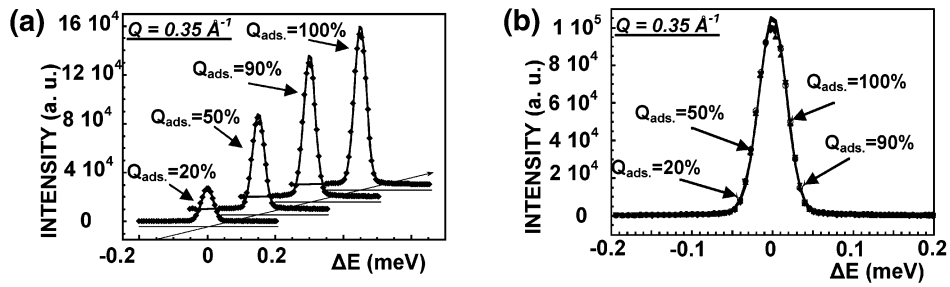

Figure 4. Measured incoherent quasi-elastic neutron scattering spectra of the H_2O confined phase in $AlPO_4$-5 zeolite. The different water loadings (20%, 50%, 90%, and 100%) are deduced from the calibration isotherm (Figure 3). (a) Intensity comparison of the different spectra. (b) Normalized spectra to an arbitrary value of 10^3.

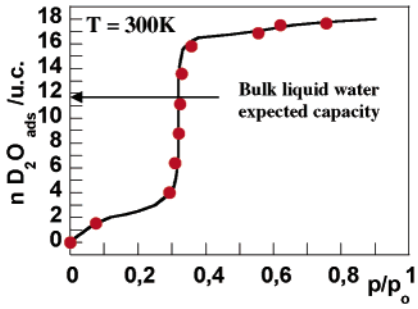

Figure 5. Calibration sorption isotherm measured at $T = 300$ K during the neutron diffraction experiment concerning the $D_2O/AlPO_4$-5 system. The full circle (red ●) represents the water loading (Q_{ads}) corresponding to the recorded diffraction patterns. Note that near 11.7 D_2O/uc of bulk liquid water is expected to fill the $AlPO_4$-5 main channels (Ø = 7.3 Å).

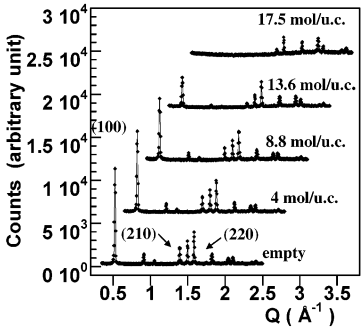

Figure 6. Experimental neutron diffraction patterns of D_2O sorbed molecules in $AlPO_4$-5 at $T = 300$ K recorded for increasing D_2O loadings.

The diffractograms were analyzed by the Rietveld method using the Fullprof[28] program. The diffractogram of the empty $AlPO_4$-5 was refined from the $AlPO_4$-5 atom coordinates and the space group *P*6*cc* obtained by Bennett et al.[29] Any attempts with the other structures reported for $AlPO_4$-5[30−34] do not decrease significantly the correlation *R*-factors (Bragg *R*-factor = 6% and R_f-factor = 7%). The hexagonal unit cell parameters of our empty $AlPO_4$-5 were found to be $a = 13.771$ Å and $c = 8.378$ Å.

Diffraction Pattern Characterization. The first changes observed in the diffractograms as a function of D_2O loadings are the intensity modifications. The first intense peak (100) and the five next ones are decreasing, even though the others at higher *Q* range are increasing. Some of these intensity modifications are plotted in Figure 7. It clearly appears that the peak intensity plot is correlated with the adsorption isotherm. The (100) intensity is slightly decreasing at $Q_{ads} = 1.5$ D_2O/uc, is decreasing from $Q_{ads} = 4$ D_2O/uc, more decreasing from $Q_{ads} = 12-16$ D_2O/uc, and is constant from $Q_{ads} = 16$ D_2O/uc. Each slope change indicates a change of the $AlPO_4$-5 filling mode. The unexpected one at $Q_{ads} = 12$ D_2O/uc corresponds to a change of the filling mode in the second part of the uptake step.

The second measured modification is the variation of the unit cell parameters. As shown in Figure 8, the *a* parameter is decreasing while the *c* parameter is increasing as a function of the water loadings. It should be noted that the fine variations of the parameters are correlated with the adsorption isotherm. It appears also that the main deformation ($\Delta a/a \cong -\Delta c/c = -0.35\%$) occurs from the loading $Q_{ads} = 12$ D_2O/uc. This finding is in agreement with X-ray diffraction results reported by Meinhold and Tapp.[35] It evidences the flexibility[36] of the $AlPO_4$-5 tetrahedral framework structure itself during the sorption. The whole modifications of the unit cell parameters

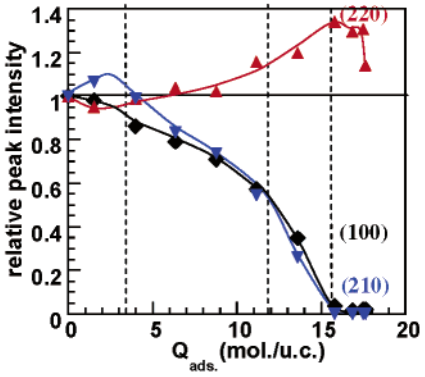

Figure 7. Relative intensity of the diffraction peaks (100) (◆), (210) (blue ▼), and (220) (red ▲) of $AlPO_4$-5 as a function of D_2O loading, determined from experimental patterns of D_2O sorbed molecules in $AlPO_4$-5 at $T = 300$ K. The dashed vertical lines separate the different filling modes.

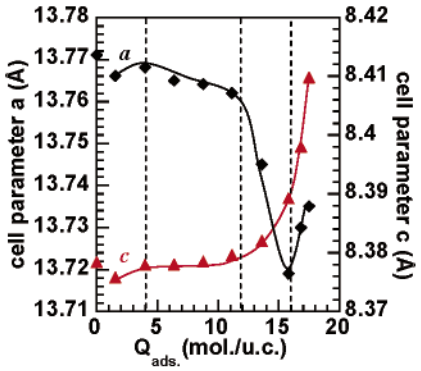

Figure 8. $AlPO_4$-5 unit cell parameter (*a* (◆) and *c* (red ▲)) as a function of D_2O loading, determined from the experimental patterns of D_2O sorbed molecules in $AlPO_4$-5 at $T = 300$ K. The dashed vertical lines separate the different filling modes.

at full loading are smaller than those observed between the 500 °C calcined sample and the as-prepared $AlPO_4$-5.[36]

Any other changes in the diffractograms are not visible. There are no additional diffraction peaks that would characterize the phase transition of the confined water. No peak shift or splitting, which would correspond to the symmetry change of the $AlPO_4$-5 structure, is observed or is resolved because of the limited nature of our neutron diffraction data.

Our first analysis of the diffractograms shows that the different filling stages evidenced from the adsorption isotherm have signatures both on the unit cell parameters and on the peak intensities.

Water Structure Simulation. The system $D_2O/AlPO_4$-5 is characterized by a high scattering length of the sorbed D_2O molecules ($b_{D2O} = 19.2 \times 10^{-13}$ cm) as compared to the $AlPO_4$-5 framework atoms ($b_{Al} = 3.4 \times 10^{-13}$ cm, $b_P = 5.1 \times 10^{-13}$ cm, $b_O = 5.8 \times 10^{-13}$ cm). Consequently, the mean location of the sorbed D_2O molecules within the $AlPO_4$-5 channel is a parameter much more sensitive toward the modification of the peak intensity of the diffraction pattern as compared to the small change of the atomic positions of the $AlPO_4$-5 framework. Therefore, before any attempt to locate the sorbed water, our first aim was to calculate the influence of water sorption on the peak intensity of the empty $AlPO_4$-5 diffractogram.

From a recent study,[17] at the initial stage ($Q_{ads} = 0-4$ D_2O/uc), the water sorption was assumed to occur in the 6-membered hexagonal nanopore as is schematically shown in Figure 9a. The resultant calculated diffractogram is given in Figure 9b and

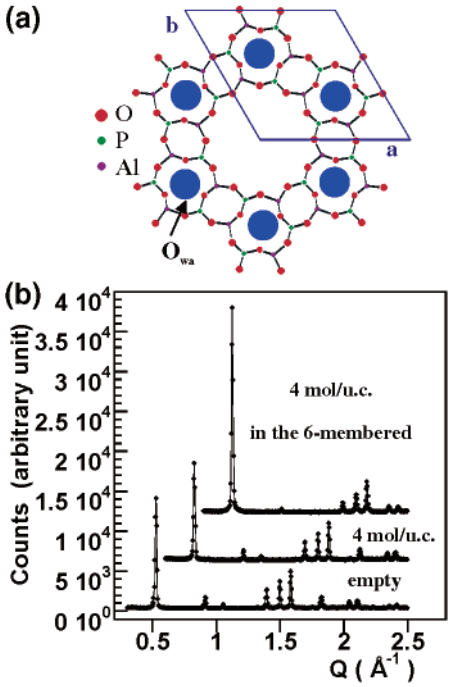

Figure 9. (a) Schematic representation of the water location in the 6-membered ring channel of $AlPO_4$-5 (Ow_a). (b) Experimental neutron diffraction patterns of the empty $AlPO_4$-5 and at the loading $Q_{ads} = 4$ D_2O/uc as compared to the calculated pattern for 4 D_2O/uc located in the 6-membered ring channel.

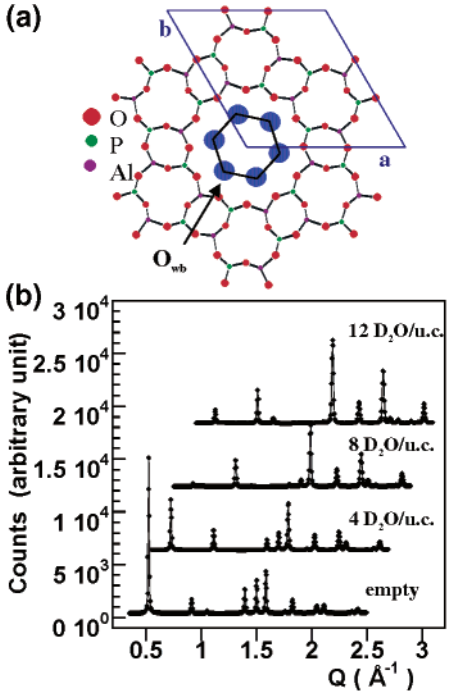

Figure 10. (a) Schematic representation of the water hexamers in the 12-membered ring channel of $AlPO_4$-5 (Ow_b). (b) Calculated neutron diffraction patterns for increasing loadings of D_2O located in the 12-membered ring channel as represented in (a).

is compared to the experimental diffractograms measured for empty $AlPO_4$-5 and at $Q_{ads} = 4$ D_2O/uc. The calculation clearly points out that the D_2O confinement in the secondary hexagonal nanopore of $AlPO_4$-5 strongly increases the (100) peak intensity (up to 2 times), whereas its measured intensity is slightly decreasing. Consequently, this recent conjecture[13,17] about an initial sorption of 4 molecules of water in the 6-membered hexagonal $AlPO_4$-5 nanopores has to be ruled out.

The uptake step ($Q_{ads} = 4-16$ D_2O/uc or $Q_{ads,cap} = 0-12$ D_2O/uc) is generally explained by the sorption of water in the main 12-membered hexagonal channel. Considering the dimensions and the hexagonal framework of the 12-membered channel of $AlPO_4$-5, two main configurations could be assumed for the water confinement. Twelve water molecules form two D_2O hexagonal rings at levels $c = {}^1/_4$ and $c = {}^3/_4$ as represented in Figure 10a. Six additional water molecules form D_2O trimers between each D_2O hexagonal ring at levels $c = 0$ and $c = {}^1/_2$ as shown in Figure 11a. The diffractograms calculated for both of these types of water confinement are plotted in Figures 10b and 11b, respectively. In both of these cases, the D_2O confinement in the main 12-membered channels of $AlPO_4$-5 induces significant and specific modifications on the peak intensity of the $AlPO_4$-5 diffractogram. At the same D_2O loading, these modifications are clearly distinguishable from one confinement to the other. However, the intensity of the first (100) peak follows a similar evolution reported in Figure 12: it is decreasing down to zero at $Q_{ads,cap} = 9$ D_2O/uc and $Q_{ads,cap} = 7$ D_2O/uc, respectively, then it is increasing. The simulation clearly points out that the confinement of an average of 8 D_2O molecules in the main hexagonal channel of $AlPO_4$-5 causes the (100) peak intensity to vanish. This is not in agreement with the measured diffractograms, because the (100) peak intensity is only half decreasing at $Q_{ads,cap} = 8$ D_2O/uc and reaches its minimum at $Q_{ads,cap} = 12$ D_2O/uc. This calculation evidences that all of the water molecules sorbed within the uptake step phenomenon are not exclusively confined in the main 12-membered channels of $AlPO_4$-5. In light of these findings, the simulation of a third arrangement is calculated. In that case, the water molecules are confined in both types of the $AlPO_4$-5 channels as represented in Figure 13a.

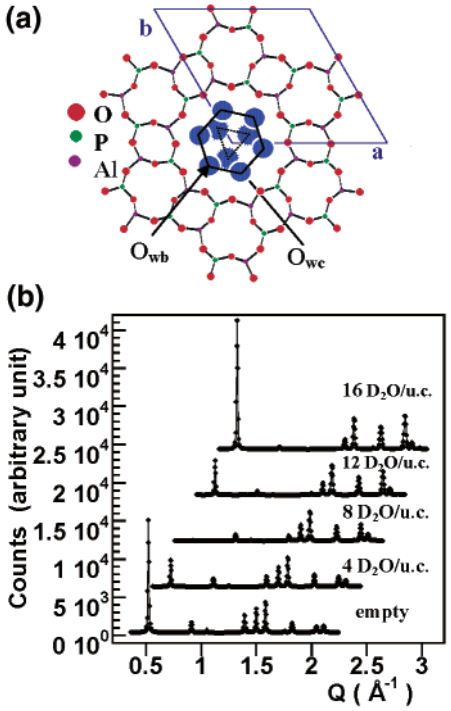

Figure 11. (a) Schematic representation of the water hexamers and trimers in the 12-membered ring channel of $AlPO_4$-5. (b) Calculated neutron diffraction patterns for increasing loadings of D_2O located in the 12-membered ring channel as represented in (a). D_2O occupation is proportional to $2Ow_b$ and $1Ow_c$ for every loading.

The calculated diffractograms are shown in Figure 13b, and the intensity of the (100) peak is plotted in Figure 12. It could be seen that, as expected, the (100) peak intensity decreases

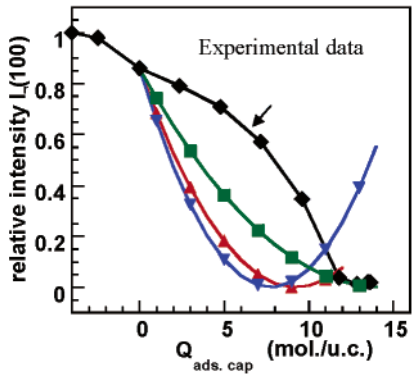

Figure 12. Relative intensity of the diffraction peak (100)$AlPO_4$-5 as a function of D_2O loading, determined from the experimental patterns of $D_2O/AlPO_4$-5 at $T = 300$ K (◆), and the patterns calculated in Figure 9 (red ▲), in Figure 10 (blue ▼), and in Figure 12 (green ■), respectively.

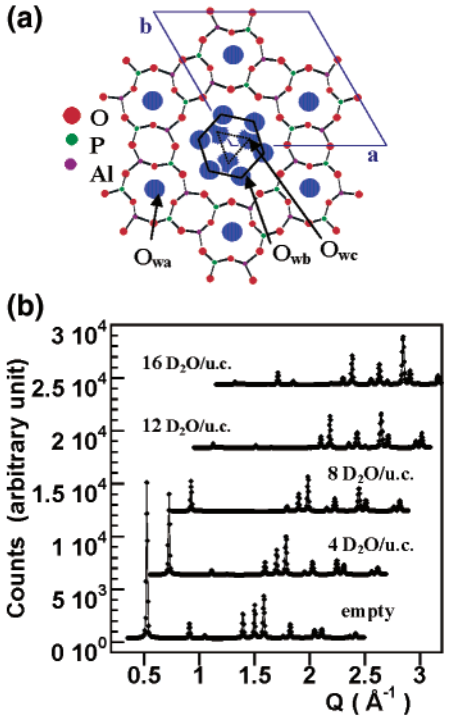

Figure 13. (a) Schematic representation of the water location in the 6- and 12-membered ring channels of $AlPO_4$-5. (b) Calculated neutron diffraction patterns for increasing loadings of D_2O located in both $AlPO_4$-5 channels as represented in (a). D_2O occupation is proportional to $1Ow_a$, $2Ow_b$, and $1Ow_c$ for every loading.

down to zero at higher loading, at $Q_{ads,cap} = 12$ D_2O/uc. Yet, there is still a large disagreement with the measured diffractograms at lower loadings.

The above analysis highlights that reliable interpretations based on the global analysis of experimental and theoretical works could be wrong. Furthermore, it appears that the experimental diffractograms measured at each step of the isotherm sorption are necessary to avoid misinterpretations of the confinement process of the sorbed molecules.

Water Structure Determination. Our second analysis of the diffractograms is to determine the location of the water molecules inside the $AlPO_4$-5 nanopores at each step of the adsorption. The diffractograms were analyzed using the Fullprof[28] program by applying the methodology described previously for the sorption of benzene in Silicalite-1.[37] The coordinates of the $AlPO_4$-5 framework atoms are restrained; the D_2O sorbed molecules are in free rotation from their O center that is allowed to move during the refinement (SPHS-type (spherical harmonic symmetry) form-factor is used for D_2O). Actually, within the resolution of our data, the correlation *R*-factors do not change significantly for rigid body refinements (D_2O molecule has a fixed geometry water (distance OD = 0.98 Å, angle DOD = 109°) and is allowed to move and to rotate from its O center).

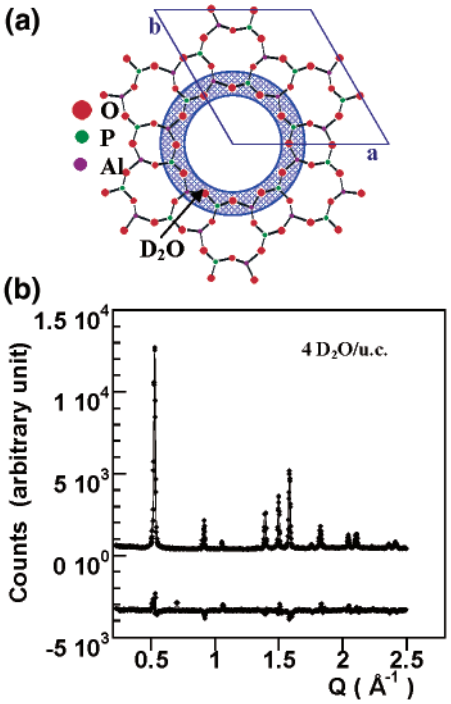

Figure 14. (a) Schematic representation of the 4-water location on the inner wall of the 12-membered ring channel of $AlPO_4$-5. (b) Experimental neutron diffraction patterns at the loading $Q_{ads} = 4$ D_2O/uc: the fitted pattern corresponding to the 4-water location represented in (a) and the difference pattern.

At the initial stage, at the low loading $Q_{ads} = 1.5-4$ D_2O/uc, D_2O molecules always converge to positions close to the walls of the main $AlPO_4$-5 channel as represented in Figure 14a. The diffractograms (Figure 14b) are well fitted, with good correlation *R*-factors (Bragg *R*-factor = 16% and R_f-factor = 11%) for water molecules (Ow_1) setting at an acceptable distance from the O atoms ($O-Ow_1 > 2.5$ Å), or at a mean distance from the Al atoms such as $Al-Ow_1 \approx 2$ Å. Only additional analysis could help us to choose among these different water positions. However, this result confirms that, as is generally reported,[13,16,35,38] the first D_2O molecule adsorption occurs on structural defects[16,39] or on Al atoms (up to 4.8 Al/uc)[38] by forming octahedral coordination.[11,12] Furthermore, such static arrangement of these bound water molecules is in agreement with our IQENS results.

Within the vertical uptake step, at loadings from $Q_{ads} = 4-16$ D_2O/uc, the refinement leads invariably to water positions within the main and the secondary channels of $AlPO_4$-5 as is expected from the above simulations. Numerous experimental and theoretical structures of bulk and confined water were tested.

The initial water positions as well the constraints on distances and angles between them and $AlPO_4$-5 atoms were chosen according to known structures of water and those determined in zeolite (lindeL, mazzite, wairakite, bikitaite) and in crystalline aluminophosphates (metavariscite, $AlPO_4$-H_3, $AlPO_4$-8, VPI-5). Finally, only one acceptable fit of each diffractogram is obtained for water positions initially chosen from a comparison

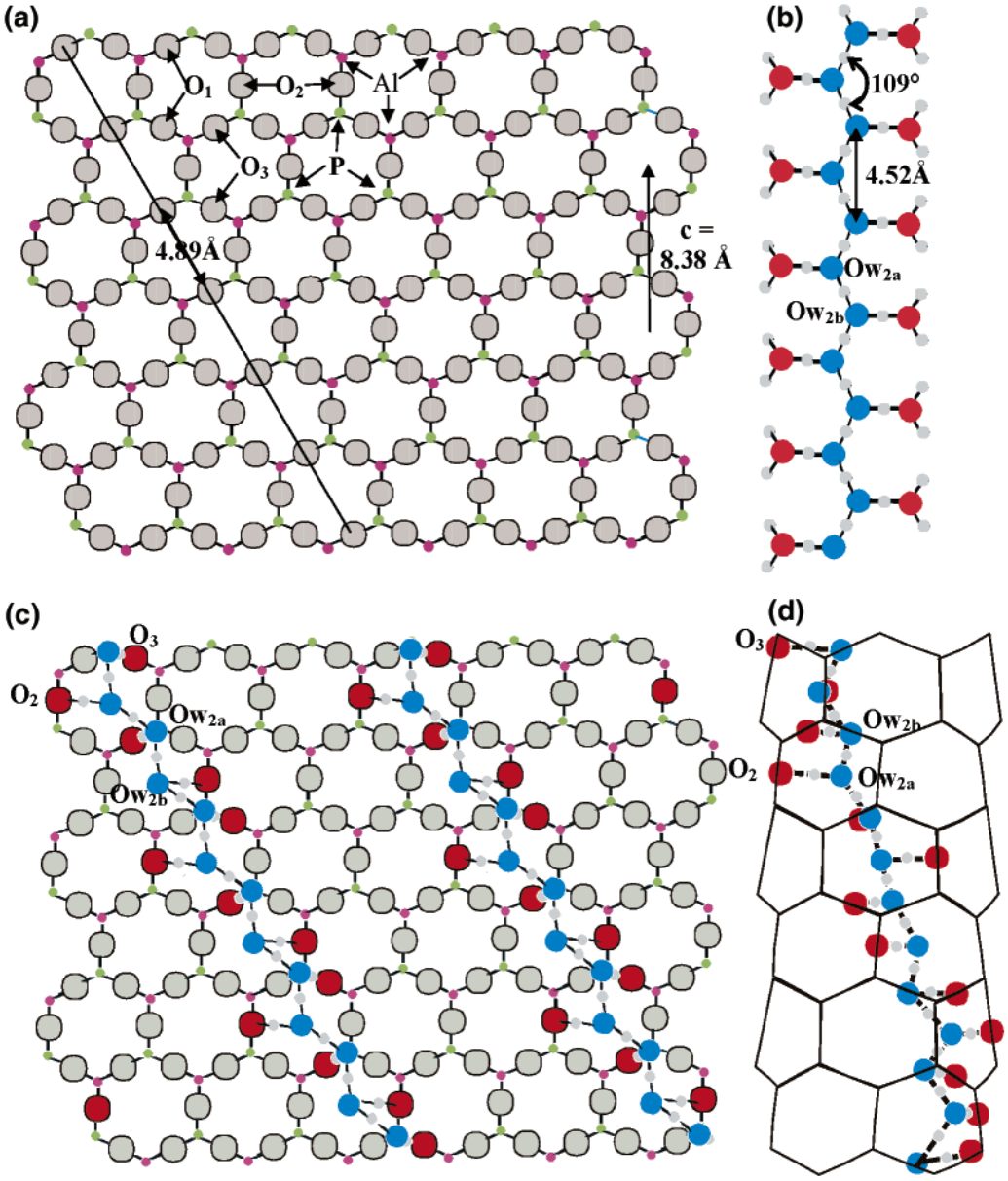

Figure 15. Schematic representations of (a) the developed inner surface of the main $AlPO_4$-5 channel; (b) a chain of water in the hexagonal ice structure; (c) the epitaxial arrangement of two chains of water on the developed inner surface of the main $AlPO_4$-5 channel; and (d) the helical arrangement of one chain of water as in (b), H-bonded with the oxygens of the inner surface of the main $AlPO_4$-5 channel.

between the hexagonal ice structure and the $AlPO_4$-5 framework. Thus, the developed inner surface of the main $AlPO_4$-5 channel (Figure 15a) is a hexagonal network of oxygen having a unit cell parameter of 4.89 Å. A chain of water molecules arranged in the hexagonal ice structure (Figure 15b) has a similar parameter of 4.52 Å. This structural comparison shows that two chains of water molecules could be H-bonding with the inner surface oxygens by involving small angular deformation (±10°) (Figure 15c). Note that these two chains of 12 water molecules each will form two helices of water inside the $AlPO_4$-5 channels (Figure 15d). Such a helical arrangement of the water molecules in $AlPO_4$-5 is comparable to the triple helix of water inside VPI-5.[10,11] Furthermore, the molecular dynamics study of the structure and dynamics of water in cylindrical pores by Hartnig et al.[40] predicted the formation of rigid helical structures of water in nanopores with diameters less than about 10 Å.

For the first part of the uptake step, from $Q_{ads} = 4-12$ D_2O/uc, the diffractogram refinement leads to two types of water location.

Figure 16b shows the experimental diffraction pattern and the calculated pattern corresponding to the correlation *R*-factors: Bragg *R*-factor = 16% and R_f-factor = 12%. Four molecules (Ow_1) are located inside the hexagonal opening between the main and secondary channels. Eight molecules (Ow_{2a} and Ow_{2b}) form two helices commensurate with the inner structure of the $AlPO_4$-5 main channel. Their positions and selected interatomic distances and angles are given in Table 1. All calculated distances and angles are within the acceptable limits for H-bonding. The structure network of one helix of water within the $AlPO_4$-5 channel is drawn in Figure 16a.

For the second part of the uptake step, from $Q_{ads} = 12-16$ D_2O/uc, the refinement converges to the correlation Bragg *R*-factor = 20% and R_f-factor = 14%. The experimental and calculated patterns are shown in Figure 17b. The four added water (Ow_3) molecules are located at the H-bond distance and angle from the water (Ow_{2b}), both being on the same diameter cylinder within the $AlPO_4$-5 channel (see the drawing in Figure 16a). The previous water molecules (Ow_1, Ow_{2a}, Ow_{2b}) are

TABLE 1: Confined Water Coordinates in the $AlPO_4$-5 Hexagonal Structure[29] and Selected Interatomic Distances and Angles between Water and the Atoms of the $AlPO_4$-5 Framework Obtained from Diffractogram Refinement at the Loading Q_{ads} = 4−12 D_2O/uc

coordinates	x	y	z	angles and distances	
Ow_1	0.5493	0.1472	0.3333	$d(Ow_1-Al) = 1.931$ Å	$d(Ow_{2b}-Ow_{2a}) = 2.777$ Å
Ow_{2a}	0.3235	0.0867	0.3333	$d(Ow_1-O1) = 2.757$ Å	$d(Ow_{2b}-Ow_{2a}) = 2.773$ Å
Ow_{2b}	0.1707	0.0000	0.0830	$d(Ow_1-O4) = 2.760$ Å	$(Ow_1-Ow_{2b}-Ow_{2a}) = 128.30°$
				$d(Ow_1-Ow_{2a}) = 2.782$ Å	$(Ow_{2b}-Ow_{2a}-Ow_{2b}) = 97.81°$
				$(O4-Ow_1-Ow_{2a}) = 98.48°$	$(Ow_{2a}-Ow_{2b}-Ow_{2a}) = 114.36°$

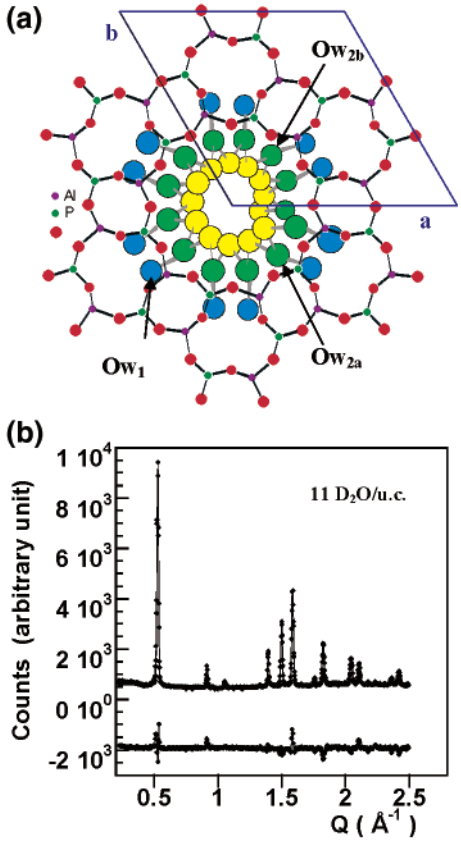

Figure 16. (a) Schematic representation of one helix of water in the 12-membered ring channel of $AlPO_4$-5. The water positions are given in Table 1. (b) Experimental neutron diffraction patterns at the loading Q_{ads} = 11 D_2O/uc: the fitted pattern corresponding to both water helices and the difference pattern.

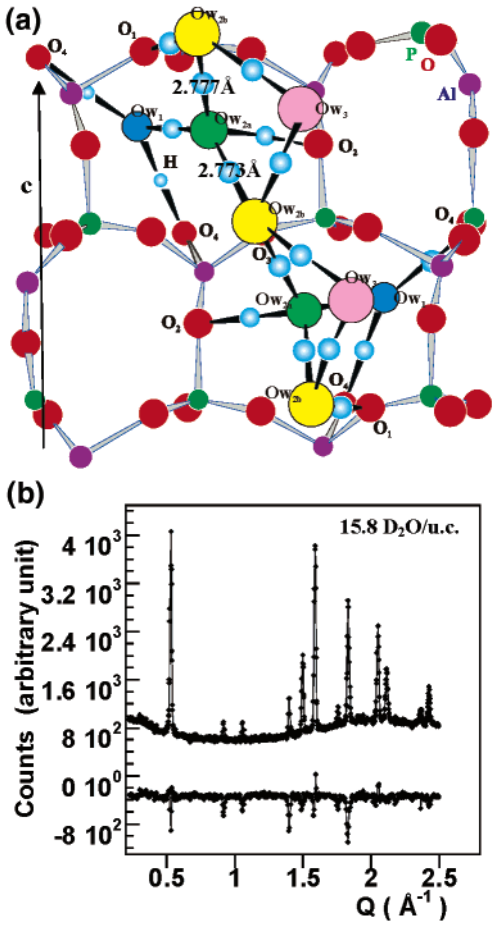

Figure 17. (a) Schematic representation of one water helix in the 12-membered ring channel of $AlPO_4$-5. The water positions are given in Table 2. (b) Experimental neutron diffraction patterns at the loading Q_{ads} = 15.8 D_2O/uc: the fitted pattern corresponding to both water helices and the difference pattern.

slightly displaced. Thus, the water Ow_1 is slightly shifted within the hexagonal opening toward the secondary channel. Also, each water helix ($Ow_{2a}-Ow_{2b}$) is slightly translated along the channel axis. Their positions and selected interatomic distances and angles are given in Table 2. The drawing in Figure 17a represents the structure network of one helix of water within the $AlPO_4$-5 channel.

Thus, the entire uptake step of the water sorption isotherm corresponds to the growth of the two helices of water, each structure of which is commensurable to the $AlPO_4$-5 channel network (represented in Figure 18). Furthermore, the ice-like character of such a helical arrangement due to the H-bond network agrees with the above-reported IQENS results.

At the final stage, at the loading Q_{ads} = 16−18 D_2O/uc, several possible locations for the two added water molecules inside the main $AlPO_4$-5 channel could be find. Yet, no clear preference for any water location could be given. Actually at Q_{ads} = 16 D_2O/uc, the main $AlPO_4$-5 channel is already full of two helices of water with which the two added water could be H-bonding. The experimental and calculated patterns (Bragg R-factor = 27% and R_f-factor = 17%) are shown in Figure 19.

At this 95% water loading, the background intensity of the experimental patterns is modified by a broad bump peaking at Q = 2.1 $Å^{-1}$ shown in Figure 20. Such broad intensity is the signature of the confined D_2O ice-like phase, the widened shape being due to nanometer size effects. However, because of its similarity in shape and position with the neutron scattering obtained from liquid D_2O at T = 300 K in the same sample holder, the absence of liquid D_2O on the outer surface of the $AlPO_4$-5 sample was checked by decreasing the temperature down to T = 273 K: there is no new diffraction peak characterizing the bulk hexagonal structure of D_2O ice. Note that such a diffraction bump was previously observed for other confined phases in $AlPO_4$-5 such as Ar,[36] D_2, and CD_4.

4. Conclusions

The global analysis of the experimental neutron data reported in this paper allowed us to elucidate the outstanding sorption behavior of water inside the $AlPO_4$-5 channels at each step of

TABLE 2: Confined Water Coordinates in the $AlPO_4$-5 Hexagonal Structure[29] and Selected Interatomic Distances and Angles between Water and the Atoms of the $AlPO_4$-5 Framework Obtained from Diffractogram Refinement at the Loading Q_{ads} = 12−16 D_2O/uc

coordinates	x	y	z	angles and distances	
Ow_1	0.6028	0.2441	0.3176	$d(Ow_1-O1) = 2.799$ Å	$d(Ow_{2b}-Ow_{2a}) = 2.773$ Å
Ow_{2a}	0.3235	0.0859	0.2824	$d(Ow_1-O4) = 2.822$ Å	$d(Ow_3-Ow_{2b}) = 2.797$ Å
Ow_{2b}	0.1772	0.0475	0.0324	$d(Ow_{2a}-O2) = 2.912$ Å	$(Ow_{2b}-Ow_{2a}-Ow_{2b}) = 98.35°$
Ow_3	0.1896	0.0526	0.2466	$d(Ow_{2b}-O1) = 2.756$ Å	$(Ow_{2a}-Ow_{2b}-Ow_{2a}) = 111.56°$
				$d(Ow_{2b}-O3) = 2.729$ Å	$(Ow_{2a}-Ow_{2b}-Ow_3) = 120.80°$
				$d(Ow_{2b}-Ow_{2a}) = 2.777$ Å	

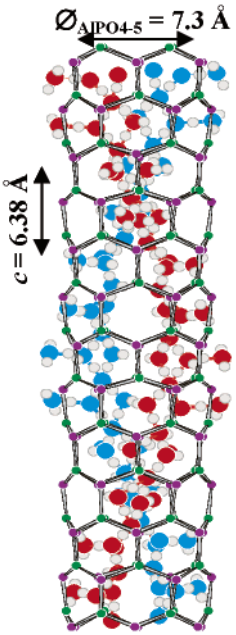

Figure 18. Schematic representation of each helix of water in the 12-membered ring channel of $AlPO_4$-5.

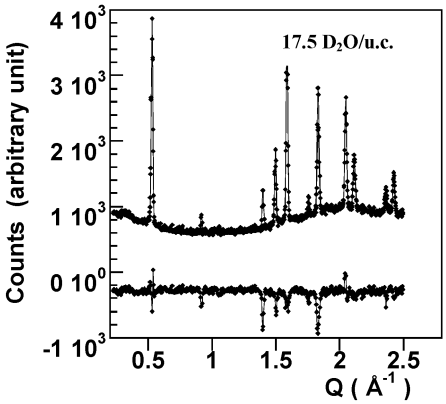

Figure 19. Experimental neutron diffraction patterns at the loading Q_{ads} = 17.5 D_2O/uc: the fitted pattern and the difference pattern.

the sorption. Thus, at low relative pressure $p/p_0 \ll 0.1$, the $AlPO_4$-5 channels remain empty of water molecules, as is expected for hydrophobic channels. Up to $p/p_0 = 0.35$, the only water molecules entering are those interacting with framework aluminum in octahedral coordination or with defects. At $p/p_0 = 0.35$, water molecules fill the $AlPO_4$-5 channels; at $p/p_0 = 0.35$, the growth of two helices of water starts from the initial sorbed water and is driven by structural commensurability with the $AlPO_4$-5 channel structure. Above $p/p_0 = 0.35$, the confined ice-like phase reaches a density of 1.2.

Such a water sorption mechanism explains the dramatic change in water sorption behavior: the so-called "capillary condensation" or the "wet−dry transition". In fact, the vertical

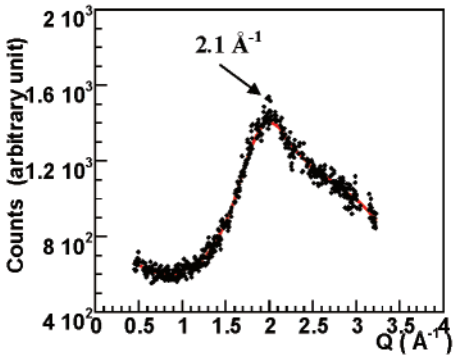

Figure 20. Background of the experimental neutron diffraction pattern recorded at $T = 300$ K and at the loading $Q_{ads} = 17.5$ D_2O/uc given in Figure 19. The diffraction from the empty $AlPO_4$-5 has been subtracted off.

step observed for adsorption of water in $AlPO_4$-5 at 300 K is proved to be the crystallization of water in two helices of ice. In this particular system, the verticality of the step refers to the constant chemical potential of the water crystallization in $AlPO_4$-5 at room temperature. This result could be related to the adsorption phenomena observed in the bidimensional systems.

The dense ice-like properties of the confined water at $T = 300$ K are related to the hydrogen-bond network that makes each water helix commensurable with the $AlPO_4$-5 channel framework. Actually, in the case of porous materials made of amorphous SiO_2, the confined water is liquid at $T = 300$ K and at much lower temperature such as $T = 215$ K for D_2O confined in MCM-41 (Ø = 19 Å).[4,6] Our finding would provide an answer for the theoretical calculations published by Hartnig et al., by giving evidence that structural commensurability effects are prevailing in the helical structure water growth in the case of the $AlPO_4$-5 nanopore. On the contrary, no helical water structures except solid-like ordered structures (such as pentagonal arrangement) were predicted in the case of water confined in a hydrophobic channel[41] and in carbon nanotubes.[21,42] Thus, the different theoretical approaches carried out on the water confinement generally well concluded the low diffusivity of the water confined in the nanotube. However, the modeling of the water structure and ordering could be reviewed in the light of our experimental results.

Furthermore, the arrangement of water molecules inside the $AlPO_4$-5 channels in a double helical structure provides an attractive interpretation of all our experimental data and is in good agreement with experimental results previously reported. However, new experimental investigations such as X-ray diffraction and IR spectroscopy analyses are underway to confirm and refine our findings.

References and Notes

(1) Dore, J. D.; Weber, B.; Hartl, M.; Behrens, P.; Hansen, T. *Physica A* **2002**, *314*, 501.

(2) Llewellyn, P. L.; Schüth, F.; Grillet, Y.; Rouquerol, F.; Rouquerol, J.; Unger, K. K. *Langmuir* **1995**, *11*, 574.
(3) Morishige, K.; Nobuoka, K. *J. Chem. Phys.* **1997**, *107*, 6965.
(4) Floquet, N.; Coulomb, J. P.; Martin, C.; Grillet, Y.; Llewellyn, P. L.; André, G. *Proceedings of the 12th International Zeolite Conference*; Treacy, M. J.; et al., Eds.; Material Research Society: Pittsburgh, PA, 1999; p 659.
(5) Morishige, K.; Kawano, K. *J. Chem. Phys.* **1999**, *110*, 4867.
(6) Coulomb, J. P.; Floquet, N.; Grillet, Y.; Llewellyn, P. L.; Kahn, R.; André, G. *Stud. Surf. Sci. Catal.* **2000**, *128*, 235.
(7) Morishige, K.; Iwasaki, H. *Langmuir* **2003**, *19*, 2809.
(8) Takahara, S.; Nakano, M.; Kittaka, S.; Kuroda, Y.; Mori, T.; Hamano, H.; Yamaguchi, T. *J. Phys. Chem. B* **1999**, *103*, 5814.
(9) Oh, J. S.; Shim, W. G.; Lee, J. W.; Kim, J. H.; Moon, H.; Seo, G. *J. Chem. Eng. Data* **2003**, *48*, 1458.
(10) McCusker, L. B.; Baerlocher, Ch.; Jahn, E.; Bülow, M. *Zeolites* **1991**, *11*, 308.
(11) Fois, E.; Gamba, A.; Tilocca, A. *J. Phys. Chem. B* **2002**, *106*, 4806.
(12) Knops-Gerrits, P. P.; Toufar, H.; Li, X. Y.; Grobet, P.; Schoonheydt, R. A.; Jacobs, P. A.; Goddard, W. A. *J. Phys. Chem. A* **2000**, *l04*, 2410.
(13) Davis, M. E.; Montes, C.; Hathaway, P. E.; Arhancet, J. P.; Hasta, D. L.; Garces, J. M. *J. Am. Chem. Soc.* **1989**, *111*, 3919.
(14) Izmailova, S. G.; Vasiljeva, E. A.; Karetina, I. V.; Feoktistova, N. N.; Khvoshchev, S. S. *J. Colloid Interface Sci.* **1996**, *179*, 374.
(15) Malla, P. B.; Komarneni, S. *Zeolite* **1995**, *15*, 324.
(16) Tsutsumi, K.; Mizoe, K.; Chubachi, K. *Colloid Polym. Sci.* **1999**, *277*, 83.
(17) Newalkar, B. L.; Jasra, R. V.; Kamath, V.; Bhat, S. G. T. *Microporous Mesoporous Mater.* **1998**, *20*, 129.
(18) Line, C. M. B.; Kearley, G. J. *J. Chem. Phys.* **2000**, *112*, 9058.
(19) Fois, E.; Gamba, A.; Tabacchi, G.; Quartieri, S.; Vezzalini, G. *J. Phys. Chem. B* **2001**, *105*, 3012.
(20) Hummer, G.; Rasaiah, J. C.; Noworyta, J. P. *Nature* **2001**, *414*, 188.
(21) Koga, K.; Gao, G. T.; Tanaka, H.; Zeng, X. C. *Physica A* **2002**, *314*, 462.
(22) Maniwa, Y.; Kataura, H.; Abe, M.; Suzuki, S.; Achiba, Y.; Kira, H.; Matsuda, K. J. *Phys. Soc. Jpn.* **2002**, *71*, 2863.
(23) Sansom, M. S. P.; Biggin, P. C. *Nature* **2001**, *414*, 156.
(24) Barrer, R. M.; Villiger, H. *Kristallografiya* **1969**, *128*, 352.
(25) Martin, C.; Tosi-Pellenq, N.; Patarin, J.; Coulomb, J. P *Langmuir* **1998**, *14*, 1774.
(26) Coulomb, J. P.; Floquet, N.; Martin, C.; Kahn, R. *Eur. J. Phys. E* **2003**, *12*, 7.
(27) Floquet, N.; Coulomb, J. P.; Dufau, N.; Andre, G.; Kahn, R. *Physica B* **2004**, in press.
(28) Rodriguez-Carvajal, J. *ILL Internal Report*; Fullprof Computer program.
(29) Bennett, J. M.; Cohen, J. P.; Flanigen, E M.; Pluth, J. J.; Smith, J. V. *ACS Symposium Series*; American Chemical Society: Washington, DC, 1983; Vol. 218, p 109.
(30) Richardson, J. W.; Pluth, J.; Smith, J. Y. *Acta Crystallogr.* **1987**, *C43*, 1469.
(31) Qiu, S.; Pang, Q.; Kessler, H.; Guth, J. L. *Zeolites* **1989**, *8*, 440.
(32) Moro, A. J.; Fitch, A. N.; Cole, M.; Goyal, R.; Jones, R. H.; Jobic, H.; Carr, S. W. *J. Mater. Chem.* **1996**, *6*, 1831.
(33) Ikeda, T.; Miyazawa, K.; Izumi, F.; Huang, Q.; Santoro, A. *J. Phys. Chem. Solids* **1999**, *60*, 1531.
(34) Klap, G. J.; van Koningsveld, H.; Graafsma, H.; Schreurs, A. M. M. *Microporous Mesoporous Mater.* **2000**, *38*, 403.
(35) Meinhold, R. H.; Tapp, N. J. *J. Chem. Soc., Chem. Commun.* **1990**, 219.
(36) Liu, Y.; Withers, R. L.; Noren, L. *Solid State Sci.* **2003**, *5*, 427.
(37) Floquet, N.; Coulomb, J. P.; Weber, G.; Bertrand, O.; Bellat, J. P. *J. Phys. Chem. B* **2003**, *107*, 685.
(38) Fyfe, A.; Wong-Moon, K. C.; Huang, Y. *Zeolites* **1996**, *16*, 50.
(39) Endoh, A.; Mizoe, K.; Tsutsumi, K.; Tetsu, T. *J. Chem. Soc., Faraday Trans. 1* **1989**, *85*, 1327.
(40) Hartnig, C.; Witschel, W.; Spohr, E. *J. Phys. Chem. B* **1998**, *102*, 1241.
(41) Allen, T W.; Kuyucak, S.; Chung, S.-H. *J. Chem. Phys.* **1999**, *11-I*, 7985.
(42) Kogaa, K.; Gao, G. T.; Tanaka, H.; Zeng, L. C. *Nature* **2001**, *412*, 802.